Arab J Sci Eng (2013) 38:3161–3170
DOI 10.1007/s13369-012-0462-4

RESEARCH ARTICLE - MECHANICAL ENGINEERING

Optimization of Conical Micro-Diffusers and Micro-Nozzles Considering Entropy Generation

Rached Ben-Mansour · Ahmet Z. Sahin

Received: 27 September 2011 / Accepted: 3 February 2012 / Published online: 7 December 2012

Abstract Fluid flow characteristics and entropy generation in a circular diffuser/nozzle element are studied numerically. The flow is assumed to be isothermal, laminar and incompressible with constant thermo-physical properties. The velocity field, mass flow rate, and entropy generation are investigated for several half angles in combination with several values of pressure drops. The effect of diffuser half angle on the entropy generation is investigated and discussed. Furthermore, the effect of the half angle of diffuser on the diffuser efficiency and the effect on the rectification efficiency are explained. It is shown that there is an optimum operation half angle for which the diffuser efficiency has a maximum value. In the case of a micro-diffuser 1 mm long with an inlet diameter of 100 μm, the optimum half angle was found to be 2.5°. These results are based on several parametric simulations ranging from 0 to 7° half angles and covering pressure drops between 500 and 2000 Pa.

Keywords Nozzle · Diffuser · Micro-channel · Entropy generation · Fluid flow

R. Ben-Mansour (✉)
Department of Mechanical Engineering,
Massachusetts Institute of Technology,
Cambridge, MA 02139, USA
e-mail: rmansour@kfupm.edu.sa

A. Z. Sahin
Mechanical Engineering Department,
King Fahd University of Petroleum and Minerals,
Dhahran 31261, Saudi Arabia

الخلاصة

يقدم هذا البحث دراسة عددية لخصائص التدفق وتوليد الأنتروبيا في خرطوم ناشر دائري. وقد افترضنا في هذه الدراسة أنّ التدفقَ رقائقي، متوازي الحرارة، غير قابل للضغط بخصائص حرارية - فيزيائية ثابتة. وتم بحث حقل السرعة، ونسبة التدفق، وتوليد الأنتروبيا لعدة حالات مختلفة. كذلك نوقش تأثير نِصْف زاويةِ الناشر على توليد الأنتروبيا. ثم فُسّر تأثير نِصْف زاويةِ الناشر على كفاءته وعلى الكفاءةِ التصحيحية. ولقد بينا أن هناك قيمة محددة لأفضل نِصْف زاويةٍ تنتج عنها كفاءة قصوى للناشر. وفي حالة ناشر دقيق طوله مليمتر واحد، وقطره مائة ميكرومتر وجدنا أن الزاوية المفضلة درجتان ونصف. واعتمدت النتائج المقدمة على عدة محاكمات عددية تتراوح فيها نصف زاوية الناشر بين صفر وسبع درجات، ويتراوح فيها نزول الضغط بين 500 و2000 باسكال.

List of Symbols

A	Cross-sectional area (m^2)
C_p	Pressure recovery coefficient
D	Diameter (m)
K	Pressure loss coefficient
L	Length of diffuser (m)
$\dot{m}$	Mass flow rate (kg/s)
P	Pressure (Pa)
R_0	Small radius of micro-nozzle/diffuser (m)
R_1	Large radius of micro-nozzle/diffuser (m)
Q	Volumetric flow rate (m^3/s)
T_o	Ambient temperature (K)
r	Radial coordinate (m)
$\dot{S}^m_{gen}$	Volumetric entropy generation rate (W/K m^3)
$\dot{S}_{gen}$	Entropy generation rate (W/K)
V	Velocity component (m/s)
V	Velocity (m/s)
z	Axial coordinate (m)
α	Diffuser/nozzle half angle
ε	Rectification efficiency
Φ	Dissipation function

μ	Viscosity (N s/m^2)
ρ	Density (kg/m^3)
η	Diffuser/nozzle efficiency
Subscripts	
b	Backward
d	Diffuser
ex	Exit
f	Forward
in	Inlet
max	Maximum
min	Minimum
n	Nozzle
out	Outlet
r	Radial
T	Total
z	Axial

1 Introduction

Micro-electromechanical systems (MEMS) have attracted a growing research interest during the recent years. This may be due to the technological developments achieved in the area of micro- and nanotechnology. As a result, scientists have started to look into the microfluidic systems in more detail. These systems find application in chemical analysis systems, micro-dosage systems and cooling of electronic devices. One of the main components of microfluidic systems is the micropump and one of the common types of micropumps is the valve-less diffuser micropump that consists of diffuser/nozzle sections and a reservoir in which the pressure of the fluid is controlled by means of a diaphragm. The fluid flow is generated as a result of so-called "vena-contracta" effect. It is observed when reversing the pressure difference in a diffuser/nozzle segment. As the pressure difference is reversed, unequal amounts of fluid flows through the diffuser/nozzle element due to the difference in flow resistances in opposite directions. Thus, applying reversible pressure difference at certain frequency, it is possible to direct the fluid flow in one preferential direction.

A number of investigations on fluid flow characteristics in micro-diffuser/nozzle elements are found in the literature. Singhal et al. [1] studied low Reynolds number flow characteristics through gradually expanding conical and planar diffusers. They presented the pressure loss coefficient with diffuser angle and found that the pressure loss coefficients at low Reynolds number (less than 1,000) vary significantly with Reynolds number. They also found that flow rectification properties of nozzle–diffuser elements improve with increasing Reynolds number.

Del Giudice et al. [2] studied the effect of viscous dissipation and viscosity in developing laminar flows in microchannels. They found that both temperature dependence of viscosity and viscous dissipation have significant role in laminar forced convection in straight microchannels.

Olsson et al. [3] studied fluid flow in flat-walled diffuser elements for valve-less micropumps using numerical techniques. Their simulations showed that there are differences in the flow patterns for diffuser elements and nozzle elements that explain the opposite positive flow directions. They showed that the diffuser element has an ordered flow and takes advantage of the pressure recovery, in the diverging wall direction, while the nozzle element has gross flow separation in the diverging wall direction where the effective cross-sectional area is smaller. They found no significant difference in the flow pressure characteristics between turbulent and laminar flows.

Although there is a considerable amount of investigation reported in the literature on the heat transfer and fluid flow in microchannels, there are only a few papers dealing with entropy generation. In one of such works, Haddad et al. [4] studied numerically the entropy generation in fluid flow through parallel plate microchannel. The fluid flow is assumed to be steady laminar. They discussed the effect of Knudsen, Reynolds, Prandtl and Eckert numbers and the nondimensional temperature difference on entropy generation within the microchannel. They found that the entropy generation in the microchannel decreases as the Knudsen number increases. On the other hand, they observed that the entropy generation increases as the Reynolds, Prantdl and Eckert numbers and nondimensional temperature difference increase.

In a second paper on the subject, Natarer [5] studied embedded converging surface microchannels in order to predict the entropy production in boundary layer flow with convective heat transfer. He used a similarity solution of boundary layer flow to determine entropy production for both no-slip and slip-flow regimes. He concluded that the flow past open microchannels with a slip coefficient of 2 yields a lower entropy generation. He found that the optimal Reynolds number decreased with higher temperatures, higher slip coefficients and more number of microchannels.

More recently, Zhao and Liu [6] conducted an entropy generation analysis of electro-osmotic flow in open-end and closed-end microchannels. They presented a theoretical-numerical study looking at the entropy generation in an osmotic flow in microchannels due to viscous dissipation, heat conduction and Joule heating. Furthermore, Naphon [7] conducted a study on the exergy loss of the horizontal concentric micro-fin tube heat exchanger. He presented an experimental and theoretical investigation on the entropy generation and exergy loss of a horizontal concentric micro-fin tube heat exchanger with water as the working fluid.

In the present paper, the characteristics of fluid flow and entropy generation in conical micro-diffusers and micro-noz-

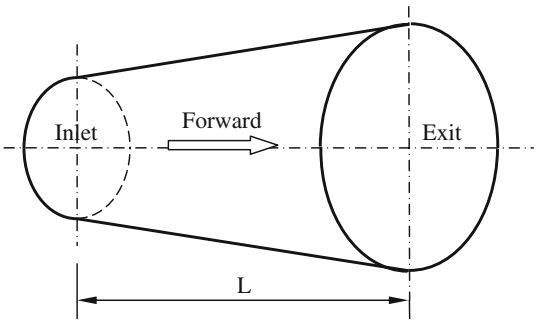

Fig. 1 Schematic diagram of conical micro-diffuser/nozzle

zles are investigated. The flow is assumed to be isothermal and laminar. The pressure loss coefficient at the inlet and outlet sections are considered in the analysis. The effect of diffuser angle on the flow rectification efficiency and diffuser/nozzle efficiency is discussed. Finally, the entropy generation within the diffuser/nozzle is studied.

2 Diffuser/Nozzle Efficiency

One of the applications of micro-diffuser/nozzle devices is in micropumps. The volume flow rate of a micropump depends on the flow rectification efficiency of the pump. It is the ability to direct the flow in one preferred direction and is defined as

$$\varepsilon = \frac{Q_{\text{net}}}{Q_{\text{f}} + Q_{\text{b}}} = \frac{Q_{\text{f}} - Q_{\text{b}}}{Q_{\text{f}} + Q_{\text{b}}} \tag{1}$$

where Q_{net} is the net flow rate in the preferred (forward) direction. Q_{b} and Q_{f} are the volumetric flow rates in the back and forward directions (Fig. 1), respectively. Fluid flow and hydrodynamics analysis are necessary for determining the volumetric flow rates.

The pressure loss in a diffuser/nozzle is given in terms of pressure loss coefficient K

$$\Delta p = K \frac{1}{2} \rho V_{\text{in}}^2 \tag{2}$$

where V_{in} is the velocity at the inlet of diffuser/nozzle. Since

$$Q = V_{\text{in}} A_{\text{in}} \tag{3}$$

$$\Delta p = K \frac{1}{2} \rho \frac{Q^2}{A_{\text{in}}^2} \tag{4}$$

or

$$Q = \sqrt{\frac{2\Delta p}{\rho}} A_{\text{in}} \frac{1}{\sqrt{K}}. \tag{5}$$

The pressure loss is the change of total pressure from the inlet to the outlet

$$\Delta p = \left(p_{\text{in}} + \frac{1}{2} \rho V_{\text{in}}^2 \right) - \left(p_{\text{out}} + \frac{1}{2} \rho V_{\text{out}}^2 \right) \tag{6}$$

Therefore, the pressure loss coefficient given in Eq. (2) can be written as

$$K = \frac{\Delta p}{\frac{1}{2} \rho V_{\text{in}}^2} = \frac{p_{\text{in}} - p_{\text{out}}}{\frac{1}{2} \rho V_{\text{in}}^2} + \left(1 - \frac{V_{\text{out}}^2}{V_{\text{in}}^2} \right) \tag{7}$$

Defining pressure recovery coefficient C_{p}

$$C_{\text{p}} = \frac{p_{\text{out}} - p_{\text{in}}}{\frac{1}{2} \rho V_{\text{in}}^2}, \tag{8}$$

the pressure loss coefficient in a conical diffuser/nozzle, Eq. (7), for incompressible flow case can be written as

$$K = 1 - \left(\frac{D_{\text{in}}^2}{D_{\text{out}}^2} \right)^2 - C_{\text{p}}. \tag{9}$$

On the other hand, the total pressure drop for a diffuser includes both the pressure loss due to sudden contraction at the inlet and the pressure loss due to sudden expansion at the exit sections:

$$\begin{aligned} \Delta p_{\text{T,d}} &= \Delta p_{\text{in,d}} + \Delta p_{\text{d}} + \Delta p_{\text{ex,d}} \\ &= K_{\text{in,d}} \frac{1}{2} \rho V_{\text{in,d}}^2 + K_{\text{d}} \frac{1}{2} \rho V_{\text{in,d}}^2 + K_{\text{ex,d}} \frac{1}{2} \rho V_{\text{ex,d}}^2 \end{aligned} \tag{10}$$

Therefore, the total pressure loss coefficient for a diffuser can be written as

$$\begin{aligned} K_{\text{T,d}} &= \frac{\Delta p_{\text{T,d}}}{\frac{1}{2} \rho V_{\text{in,d}}^2} = K_{\text{in,d}} + K_{\text{d}} + K_{\text{ex,d}} \frac{V_{\text{ex,d}}^2}{V_{\text{in,d}}^2} \\ &= K_{\text{in,d}} + K_{\text{d}} + K_{\text{ex,d}} \frac{A_{\text{in,d}}^2}{A_{\text{ex,d}}^2} \end{aligned} \tag{11}$$

Similarly for a nozzle, the total pressure loss coefficient can be written based on the pressure head at the throat (at exit) as

$$K_{\text{T},n} = \frac{\Delta p_{\text{T},n}}{\frac{1}{2} \rho V_{\text{ex},n}^2} = (K_{\text{in},n} + K_n) \frac{A_{\text{ex},n}^2}{A_{\text{in},n}^2} + K_{\text{ex},n} \tag{12}$$

It should be noted that

$$A_{\text{in,d}} = A_{\text{ex},n} = A_{\min} \quad \text{and} \quad A_{\text{ex,d}} = A_{\text{in},n} = A_{\max}.$$

Considering diffuser flow as forward and nozzle flow as the backward

$$K_{\text{f}} = K_{\text{T,d}} \quad \text{and} \quad K_{\text{b}} = K_{\text{T},n},$$

the diffuser/nozzle efficiency can be defined as the ratio of the pressure loss coefficient of nozzle (backward) to that of

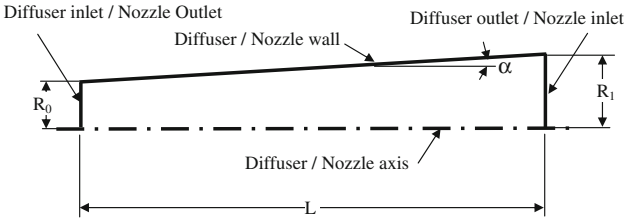

Fig. 2 Schematic of micro-conical diffuser/nozzle and design parameters: L = length, D_0 = small diameter, D_1 = large diameter, α = half angle

Table 1 Different meshes used in the grid independence study

Grid label	Number of nodes (radial, axial)	Features
M0	20 × 70	Refined[a] near wall and entrance
M1	30 × 100	Refined near wall and entrance
M2	40 × 200	Refined near wall and entrance
M3	40 × 200	Refined near wall, near axis and entrance.
.		

[a] The refinement is done using a successive ratio formula

the diffuser (forward)

$$\eta = \frac{K_\mathrm{b}}{K_\mathrm{f}} = \frac{K_{\mathrm{T},n}}{K_{\mathrm{T,d}}} = \frac{(K_{\mathrm{in},n} + K_n)\frac{A_{\min}^2}{A_{\max}^2} + K_{\mathrm{ex},n}}{K_{\mathrm{in,d}} + K_\mathrm{d} + K_{\mathrm{ex,d}}\frac{A_{\min}^2}{A_{\max}^2}} \tag{13}$$

Finally, it is worth noting that in our case the flow is isothermal and the viscous dissipation can be neglected. CFD simulations have shown that its inclusion resulted in a maximum change of 0.1 K, and therefore the head loss coefficient is the same as the exergy loss coefficient as given in Makhanlall et al. [8] and Schmandt and Herwig [9]. Hence, the energy efficiency and exergy efficiency are the same for isothermal flow conditions.

3 Flow Field Formulation

The work presented here is limited to the case of laminar flow. The Navier–Stokes equations are solved for a circular geometry of a micro-diffuser or micro-nozzle. The conical diffuser/nozzle is identified with smaller radius R_0 and larger radius R_1 as shown in Fig. 2 and a length L. Normally, we define R_0, L and the half angle α and determine R_1.

The Navier–Stokes equations for laminar steady flow can be written in cylindrical coordinates as follows. Continuity:

$$\frac{\partial v_\mathrm{r}}{\partial r} + \frac{v_\mathrm{r}}{r} + \frac{\partial v_\mathrm{z}}{\partial z} = 0 \tag{14}$$

Momentum:

$$\rho\left(v_\mathrm{r}\frac{\partial v_\mathrm{r}}{\partial r} + v_\mathrm{z}\frac{\partial v_\mathrm{r}}{\partial z}\right) = -\frac{\partial P}{\partial r} + \mu\left\{\frac{\partial}{\partial r}\left[\frac{1}{r}\frac{\partial}{\partial r}(r v_\mathrm{r})\right] + \frac{\partial^2 v_\mathrm{r}}{\partial z^2}\right\} \tag{15}$$

$$\rho\left(v_\mathrm{r}\frac{\partial v_\mathrm{z}}{\partial r} + v_\mathrm{z}\frac{\partial v_\mathrm{z}}{\partial z}\right) = -\frac{\partial P}{\partial r} + \mu\left\{\frac{1}{r}\frac{\partial}{\partial r}\left[r\frac{\partial v_\mathrm{z}}{\partial r}\right] + \frac{\partial^2 v_\mathrm{z}}{\partial z^2}\right\} \tag{16}$$

The flow boundary conditions used are as follows:

$$v_\mathrm{r} = 0, \quad v_\mathrm{z} = 0 \quad \text{at the wall of diffuser/nozzle} \tag{17}$$

$$P = \Delta P \quad \text{at } z = 0 \text{ (inlet of diffuser/nozzle)} \tag{18}$$

$$P = 0 \quad \text{at } z = L \text{ (exit of diffuser/nozzle)} \tag{19}$$

$$v_\mathrm{r} = 0, \quad \frac{\partial v_\mathrm{z}}{\partial r} = 0 \quad \text{at the axis } (r = 0, 0 < z < L).$$

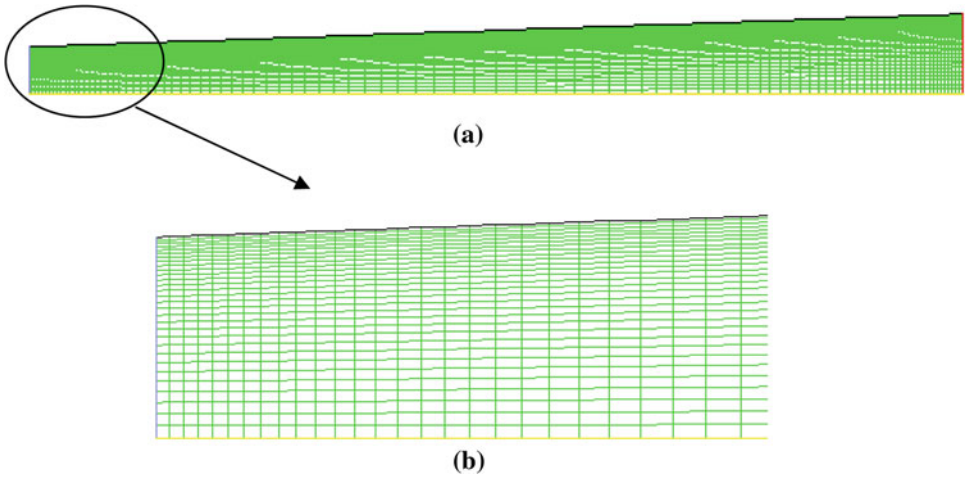

Fig. 3 Numerical mesh for the micro-diffuser with 3° half angle. **a** Entire mesh, **b** enlarged view showing mesh refinement near the wall and entry

Table 2 Computational runs and grid-independence study for the diffuser flow

Geometry				Pressure drop (Pa)			Variable	Mesh-discretization order
R_0 (mm)	L (mm)	α (°)	R_1 (mm)	$\Delta P = 500$	$\Delta P = 1,000$	$\Delta P = 2,000$		
0.1	1	0	0.0500	7.139E−08	1.275E−07	2.179E−07	$\dot{m}$	M1-1st order
				7.143E−08	1.276E−07	2.181E−07	$\dot{m}$	M1-2nd order
				5.081E+01	9.074E+01	1.550E+02	Re	
				8.740E−08	2.831E−07	8.463E−07	$\dot{S}_{\text{gen}}$	M1-1st order
				8.754E−08	2.838E−07	8.496E−07	$\dot{S}_{\text{gen}}$	M1- 2nd order
0.1	1	2	0.0849	1.719E−07	2.902E−07	4.696E−07	$\dot{m}$	M1-1st order
				1.729E−07	2.922E−07	4.728E−07	$\dot{m}$	M1- 2nd order
				1.223E+02	2.065E+02	3.342E+02	Re	
				2.111E−07	6.393E−07	1.791E−06	$\dot{S}_{\text{gen}}$	M1-1st order
				2.147E−07	6.530E−07	1.834E−06	$\dot{S}_{\text{gen}}$	M1- 2nd order
0.1	1	3	0.1024	2.126E−07	3.477E−07	5.478E−07	$\dot{m}$	M1-1st order
				2.145E−07	3.506E−07	5.514E−07	$\dot{m}$	M1-2nd order
				1.513E+02	2.475E+02	3.898E+02	Re	
				2.596E−07	7.531E−07	2.034E−06	$\dot{S}_{\text{gen}}$	M1-1st order
				2.668E−07	7.765E−07	2.103E−06	$\dot{S}_{\text{gen}}$	M1-2nd order
0.1	1	4	0.1199	2.458E−07	3.904E−07	6.008E−07	$\dot{m}$	M1-1st order
				2.482E−07	3.934E−07	6.033E−07	$\dot{m}$	M1-2nd order
				1.749E+02	2.779E+02	4.276E+02	*Re*	
				2.955E−07	8.228E−07	2.150E−06	$\dot{S}_{\text{gen}}$	M1- 1st order
				3.064E−07	8.549E−07	2.236E−06	$\dot{S}_{\text{gen}}$	M1-2nd order
0.1	1	5	0.1375	2.687E−07	4.179E−07	6.324E−07	$\dot{m}$	M1-1st order
				2.712E−07	4.202E−07	6.329E−07	$\dot{m}$	M1-2nd order
				2.714E−07	4.203E−07	6.326E−07	$\dot{m}$	M0-2nd order
					4.201E−07		$\dot{m}$	M2-2nd order
					4.202E−07		$\dot{m}$	M3-2nd order
				1.912E+02	2.974E+02	4.501E+02	Re	
				3.166E−07	8.543E−07	2.177E−06	$\dot{S}_{\text{gen}}$	M1-1st order
				3.305E−07	8.925E−07	2.275E−06	$\dot{S}_{\text{gen}}$	M1-2nd order
				3.302E−07	8.903E−07	2.264E−06	$\dot{S}_{\text{gen}}$	M0-2nd order
					8.939E−07		$\dot{S}_{\text{gen}}$	M2-2nd order
					8.967E−07		$\dot{S}_{\text{gen}}$	M3-2nd order
0.1	1	7	0.1728	2.991E−07	4.516E−07	6.680E−07	$\dot{m}$	M1- 1st order
				3.009E−07	4.516E−07	6.636E−07	$\dot{m}$	M1-2nd order
				2.129E+02	3.214E+02	4.754E+02	Re	
				3.349E−07	8.626E−07	2.121E−06	$\dot{S}_{\text{gen}}$	M1-1st order
				3.531E−07	9.091E−07	2.235E−06	$\dot{S}_{\text{gen}}$	M1-2nd order

4 Entropy Generation

The entropy generation rate for viscous fluid flow without heat transfer can be written as [10]:

$$\dot{S}'''_{\text{gen}} = \frac{\mu}{T_0}\Phi \tag{20}$$

The viscous dissipation is neglected in the energy equation and hence the fluid stays at the same temperature T_0. The dissipation function used for the entropy generation is given by

$$\Phi = 2\left[\left(\frac{\partial v_{\text{r}}}{\partial r}\right)^2 + \left(\frac{v_{\text{r}}}{r}\right)^2 + \left(\frac{\partial v_{\text{z}}}{\partial z}\right)^2\right] + \left(\frac{\partial v_{\text{r}}}{\partial z} + \frac{\partial v_{\text{z}}}{\partial r}\right)^2 \tag{21}$$

Table 3 Computational runs and grid-independence study for the nozzle flow

Geometry				Pressure drop (Pa)			Variable	Mesh-discretization order
R_0 (mm)	L (mm)	α (°)	R_1 (mm)	$\Delta P = 500$	$\Delta P = 1000$	$\Delta P = 2000$		
0.05	1	0	0.0500	7.139E−08	1.275E−07	2.179E−07	$\dot{m}$	M1-1st order
				7.143E−08	1.276E−07	2.181E−07	$\dot{m}$	M1-2nd order
				5.081E+01	9.074E+01	1.550E+02	Re	
				8.740E−08	2.831E−07	8.463E−07	$\dot{S}_{\text{gen}}$	M1-1st order
				8.754E−08	2.838E−07	8.496E−07	$\dot{S}_{\text{gen}}$	M1-2nd order
0.05	1	2	0.0849	1.302E−07	2.114E−07	3.338E−07	$\dot{m}$	M1-1st order
				1.303E−07	2.116E−07	3.341E−07	$\dot{m}$	M1-2nd order
				9.263E+01	1.505E+02	2.376E+02	Re	
				1.122E−07	3.050E−07	7.959E−07	$\dot{S}_{\text{gen}}$	M1-1st order
				1.124E−07	3.056E−07	7.976E−07	$\dot{S}_{\text{gen}}$	M1-2nd order
0.05	1	3	0.1024	1.474E−07	2.339E−07	3.626E−07	$\dot{m}$	M1-1st order
				1.476E−07	2.342E−07	3.630E−07	$\dot{m}$	M1-2nd order
				1.049E+02	1.665E+02	2.580E+02	Re	
				1.096E−07	2.874E−07	7.320E−07	$\dot{S}_{\text{gen}}$	M1-1st order
				1.099E−07	2.882E−07	7.341E−07	$\dot{S}_{\text{gen}}$	M1-2nd order
0.05	1	4	0.1199	1.607E−07	2.509E−07	3.839E−07	$\dot{m}$	M1-1st order
				1.610E−07	2.514E−07	3.846E−07	$\dot{m}$	M1-2nd order
				1.144E+02	1.786E+02	2.732E+02	*Re*	
				1.047E−07	2.685E−07	6.732E−07	$\dot{S}_{\text{gen}}$	M1-1st order
				1.051E−07	2.694E−07	6.757E−07	$\dot{S}_{\text{gen}}$	M1-2nd order
0.05	1	5	0.1375	1.700E−07	2.627E−07	3.981E−07	$\dot{m}$	M1-1st order
				1.707E−07	2.635E−07	3.996E−07	$\dot{m}$	M1-2nd order
				1.210E+02	1.870E+02	2.833E+02	Re	
				9.932E−08	2.519E−07	6.241E−07	$\dot{S}_{\text{gen}}$	M1-1st order
				1.003E−07	2.536E−07	6.296E−07	$\dot{S}_{\text{gen}}$	M1-2nd order
0.05	1	7	0.1728	1.847E−07	2.808E−07	4.205E−07	$\dot{m}$	M1-1st order
				1.852E−07	2.814E−07	4.215E−07	$\dot{m}$	M1-2nd order
				2.129E+02	3.214E+02	4.754E+02	Re	
				9.060E−08	2.257E−07	5.534E−07	$\dot{S}_{\text{gen}}$	M1-1st order
				9.115E−08	2.265E−07	5.559E−07	$\dot{S}_{\text{gen}}$	M1-2nd order

Equations (7) and (8) define the entropy generation rate per unit volume at any location in the domain. This expression can be integrated over the entire domain to obtain the entropy generation rate in the pipe contraction.

$$\dot{S}_{\text{gen}} = \int_{\forall} \dot{S}'''_{\text{gen}} \mathrm{d}\forall \tag{22}$$

5 Method of Solution

The solution of the problem has been carried out by a CFD packaged software [11]. The entropy generation calculation is achieved by user-defined functions. The working fluid considered is air whose thermo-physical properties are assumed to be constant at atmospheric pressure and a temperature of 288 K. The CFD software employed uses the finite volume technique which is well documented in the literature [11]. The computational domain included half the diffuser/nozzle for symmetry reasons as shown in Fig. 2.

The grid used was constructed out of a structured mesh with 30×100 (30 intervals in the radial direction and 100 in the axial direction) quadrilateral control volumes. This grid was arrived at after an extensive grid independence study which ensured less than 1 % change in the entropy generation. The different grids used are listed in Table 1 and the final grid is shown in Fig. 3. To capture the boundary layer large gradient, smaller spacing was put close to the wall using

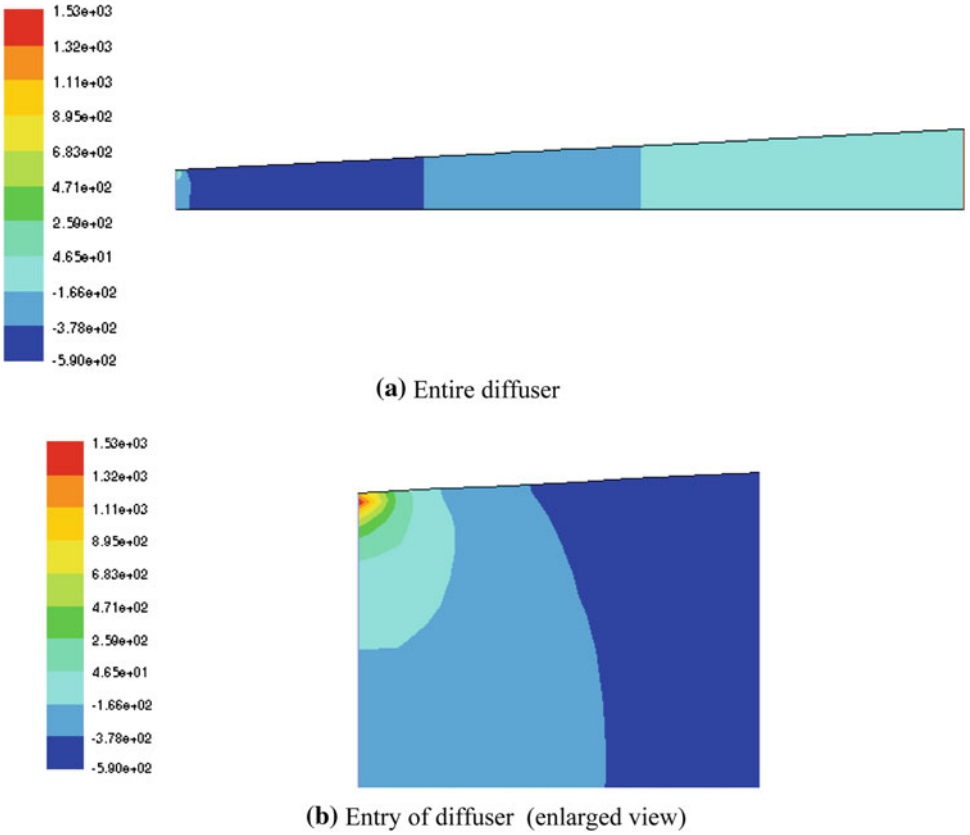

Fig. 4 Pressure contours for micro-diffuser with 3° half angle and 2 kPa pressure drop

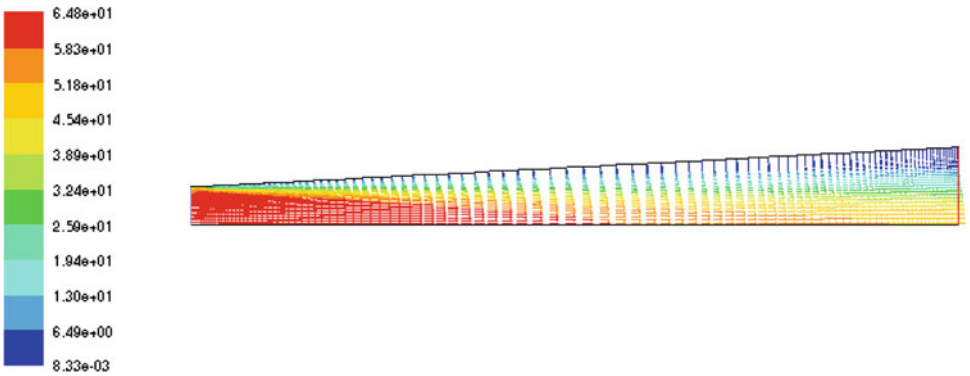

Fig. 5 Velocity vectors for micro-diffuser with 3° half angle and 2 kPa pressure drop

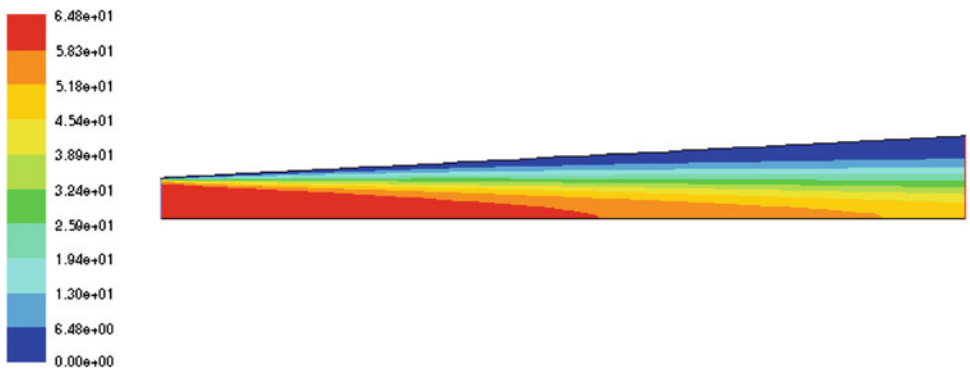

Fig. 6 Velocity magnitude in the micro-diffuser with 3° half angle and 2 kPa pressure drop

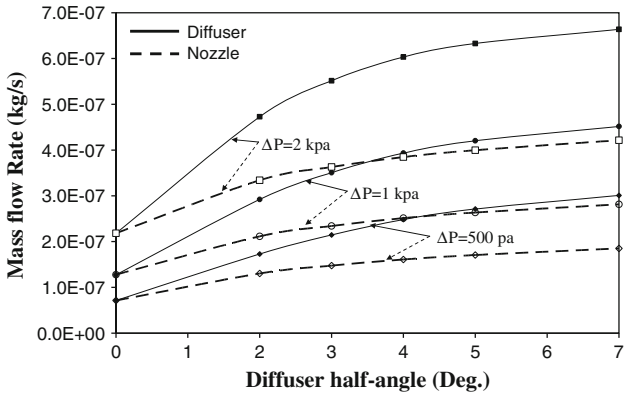

Fig. 7 Micro-diffuser and micro-nozzle mass flow rate as function of half angle for three different pressure differences

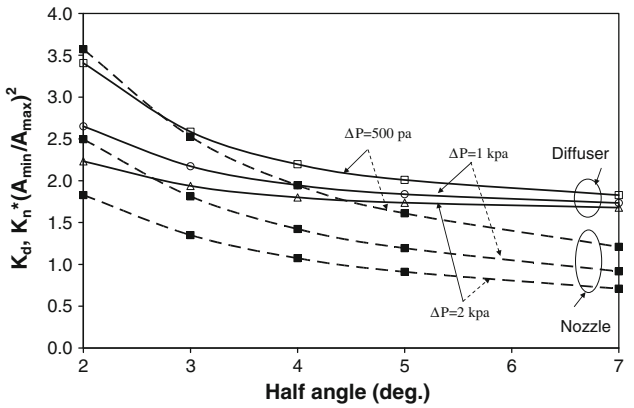

Fig. 8 Variation of diffuser and nozzle loss coefficients with half angle for three pressure differences

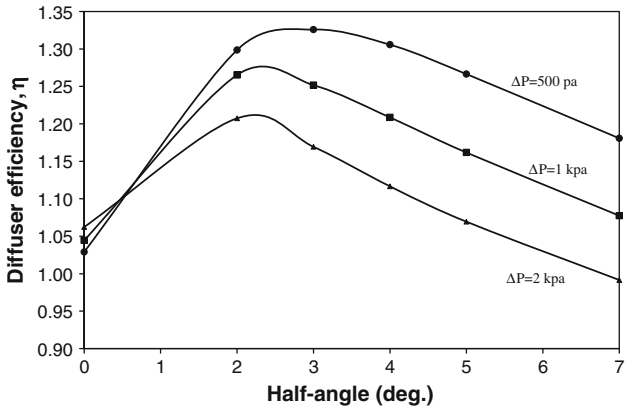

Fig. 9 Variation of micro-diffuser efficiency with half angle for three pressure differences, for rounded diffuser entrance ($K_{d,en} = 0.04$) and sharp nozzle entrance ($K_{n,en} = 0.5$)

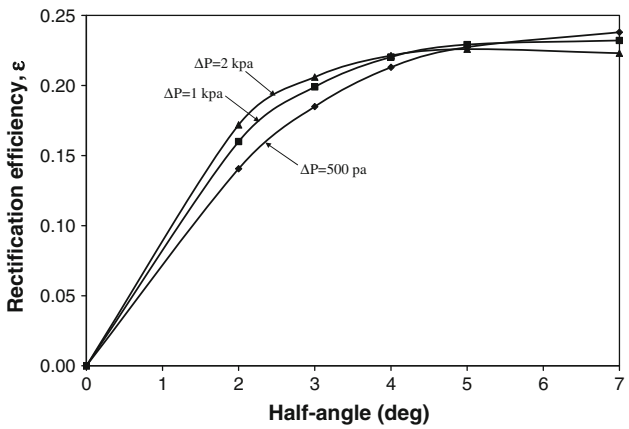

Fig. 10 Variation of micro-nozzle flow rectification efficiency with half angle for three pressure differences

a successive ratio technique. Similar refinement was done at the entry and exit of the diffuser and nozzle meshes as shown in Fig. 3.

In addition to the grid refinement, two discretization schemes were tried: the first-order upwind and second-order upwind schemes. The final results were obtained using the second-order upwind scheme for the momentum and standard scheme for the pressure. All simulations were run until the mass and momentum residuals were less than 10^{-6}. A summary of the computational runs are shown in Table 2 for the diffuser and in Table 3 for the nozzle along with the grid dependence study using five mesh sizes (see Table 1) and two discretization methods.

6 Results and Discussion

Typical flow field variables are shown in vector and contour plots to demonstrate the main features of the flow inside the diffuser or nozzles. The pressure contours inside the micro-diffuser with $D_0 = 100\,\mu$m, length $L = 1$ mm and half angle of 3° are shown in Fig. 4. A considerable pressure drop occurs in the inlet section, especially near the wall. This is due to the acceleration of the flow due to the boundary layer development in these locations. The pressure increases gradually in the downstream due to the increase of cross section of the micro-diffuser and deceleration of the flow.

The velocity vectors for 3° half angle diffuser are shown in Fig. 5 and the contours of velocity magnitude are shown in Fig. 6. The high values of the velocity gradients at the inlet of the diffuser and deceleration of the flow through the diffuser can be seen in these figures. It should also be noted that there exist no fully developed region as the flow expends continuously.

The effect of diffuser half angle on the mass flow rate for three different cases of pressure differences is given in Fig. 7. Both the forward (diffuser) and backward (nozzle) mass flow rates are shown in this figure. The difference between the mass flow rates in forward and backward directions increases as the half angle increases. However, the difference between the mass flow rates (of forward and backward direction) reaches nearly a constant value beyond a certain

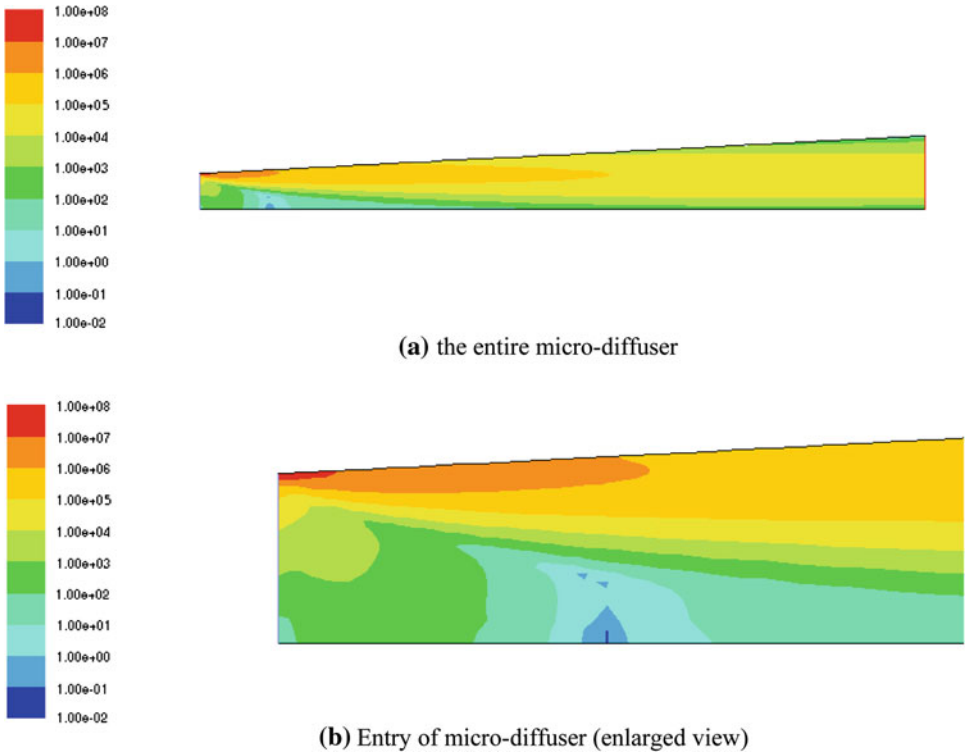

Fig. 11 Entropy generation in the micro-diffuser with 3° half angle and 2 kPa pressure drop

half angle (about 4°). As the pressure difference increases, the difference between the mass flow rates increases in general.

The effect of half angle on the pressure loss coefficients for three different pressure differences is given in Fig. 8 for both diffuser (forward) and nozzle (backward) operation. Pressure loss coefficient for both diffuser and nozzle operation decreases as the half angle increases. The reduction in the pressure loss coefficient with half angle is faster for small angles. As the half angle gets larger, the change in the pressure loss coefficient gets smaller especially for the diffuser

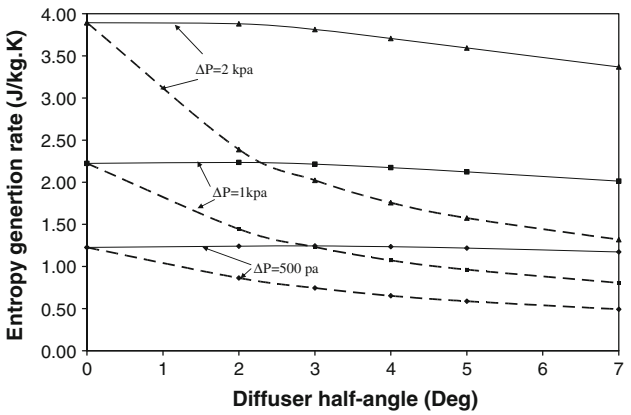

Fig. 12 Micro-diffuser and micro-nozzle entropy generation per unit mass flow rate as function of half angle for three pressure differences

case. The effect of applied pressure on the pressure drop coefficient for higher values of half angle is small. It should be noted that in Fig. 8, the inlet and exit pressure losses are not included. The less pressure loss coefficient for the case of nozzle operation for high half angle values indicates that the diffuser efficiency might get less than 1.0 as can be seen from Fig. 9.

Variation of micro-diffuser efficiency as defined by Eq. (13) is given in Fig. 9. There exists an optimum half angle for which the micro-diffuser efficiency becomes the maximum. As the pressure difference increases, the microdiffuser efficiency decreases in general. The optimum half angle decreases as the applied pressure is increased.

Figure 10 shows the micro-diffuser flow rectification efficiency defined by Eq. (1) as function of half angle. As the half angle increases, the rectification efficiency increases. The rectification efficiency approaches a steady value for higher half angles. The effect of pressure difference on the rectification efficiency, however, is negligible.

The volumetric entropy generation in the micro-diffuser is shown in Fig. 11. Entropy generation is the maximum in the entrance region, especially near the diffuser wall. This is due to the high velocity gradients occurring in these regions. In the axial direction along the micro-diffuser, the entropy generation decreases gradually. It should be noted that at an upstream location on the centerline near the inlet, the entropy

generation decreases to a minimum value. This is due to the flow acceleration as a result of boundary layer development, followed by the deceleration as a result of enlargement of the cross-sectional area of the diffuser. During this flow acceleration and deceleration process, the velocity gradients go through zero where the entropy generation decreases considerably.

The variation of entropy generation per unit mass flow rate as function of half angle is shown in Fig. 12 for three different values of pressure difference. When the pressure difference is small, the effect of the half angle on the entropy generation is negligible. However, as the applied pressure difference is increased, the effect of half angle on the entropy generation becomes important. For pressure drops higher than 1 kPa, increasing the half angle results in reducing the entropy generation. For the case of nozzle, this fact is more pronounced. The difference between the entropy generation in the forward direction and that in the backward direction increases as the half angle increases. This difference is considerably high for high pressure differences.

7 Conclusions

The flow characteristics and the entropy generation in a micro-diffuser element were studied for forward (diffuser) and backward (nozzle) operation. In this study, the micro-diffusers are 1 mm long and have an inlet diameter of a 100 μm and variable half angle. In order to obtain accurate results, fine numerical meshes and second-order discretization schemes were used. Several parametric simulations ranging from 0 to 7° half angles and covering pressure drops between 500 and 2,000 Pa were executed. Based on the results of the study, the following conclusions can be stated:

1. The boundary layer development in micro-diffuser results in acceleration of the flow near the entry of the diffuser, which is responsible for high amount of entropy generation. After the initial acceleration that occurs near the entrance, the flow decelerates along the axial direction as a result of increase in the cross-sectional area.
2. The entropy generation is the maximum at the inlet near the corner of the diffuser wall. This is due to the high velocity gradients that occur in this region. Along the axial direction, the entropy generation decreases.
3. The entropy generation decreases as the diffuser angle increases. This is due to the decrease of velocity gradients and deceleration of the flow in the diffuser.
4. The entropy generation per unit mass flow rate for backward operation (nozzle case) is less than the forward operation (diffuser case). This may be attributed to the less pressure loss coefficient in the case of nozzle operation. The mass flow rate is more in the case of diffuser operation; however, the entropy generation is also higher.
5. There exists an optimum operation half angle for which the diffuser efficiency has a maximum value.
6. For the micro-diffusers simulated in our study (1 mm long and an inlet diameter of a 100 μm), the optimum half angle was found to be 2.5°.

In our study, we considered isothermal and incompressible flow. It is recommended that future studies include flow and heat transfer in compressible flow situations.

Acknowledgments The authors would like to acknowledge the support provided by the Deanship of Scientific Research at King Fahd University of Petroleum and Minerals (KFUPM) for this work.

References

1. Singhal, V.; Garimella, S.V.; Murthy, J.Y.: Low Reynolds number flow through nozzle-diffuser elements in valveless micropumps. Sens. Actuators A **113**, 226–235 (2004)
2. Del Giudice, S.; Nonino, C.; Savino, S.: Effects of viscous dissipation and temperature dependent viscosity in thermally and simultaneously developing laminar flows in microchannels. Int. J. Heat Fluid Flow **28**, 15–27 (2007)
3. Olsson, A.; Stemme, G.; Stemme, E.: Numerical and experimental studies of flat-walled diffuser elements for valve-less micropumps. Sens. Actuators **84**, 165–175 (2000)
4. Haddad, O.; Abuzaid, M.; Al-Nimr, M.: Entropy generation due to laminar incompressible forced convection flow through parallel-plates microchannel. Entropy **6**(5), 413–426 (2004)
5. Natarer, G.F.: Embedded converging surface microchannels for minimized friction and thermal irreversibilities. Int. J. Heat Mass Transfer **48**, 1225–1235 (2005)
6. Zhao, L.; Liu, L.H.: Entropy generation analysis of electro-osmotic flow in open-end and closed-end micro-channels. Int. J. Therm. Sci. **49**, 418–427 (2010)
7. Naphon, P.: Study on the exergy loss of the horizontal concentric micro-fin tube heat exchanger. Int. Commun. Heat Mass Transfer **38**(201), 229–235
8. Makhanlall, D.; Liu, L.H.; Zhang, H.C.: Determination of loss coefficients for high-temperature flow devices: an entropy-based approach. Int. J. Therm. Sci. **49**, 1848–1855 (2010)
9. Schmandt, B.; Herwig, H.: Internal flow losses: a fresh look at old concepts. ASME J. Fluids Eng. **133**, 051201-1 (2011)
10. Bejan, A.: Entropy Generation Minimization. CRC Press, New York (1996)
11. Fluent 6 User's Guide: Fluent Inc., Lebanon (2005)
12. Patankar, S.: Numerical Heat Transfer and Fluid Flow. Hemisphere, McGraw-Hill, Washington (1980)